

## Fly Your Satellite!

---

**Analysis Report (ARPT)**

**Attitude and Orbit Control System (AOCS)**



UNIVERSITAT POLITÈCNICA  
DE CATALUNYA  
BARCELONATECH

NANOSAT LAB



**FLY YOUR SATELLITE!**

# Contents

<b>1</b>	<b>Introduction</b>	<b>9</b>
1.1	The PoCat-Lektron mission . . . . .	9
1.1.1	Mission statement . . . . .	9
1.1.2	Mission Objectives . . . . .	9
<b>2</b>	<b>Simulation model</b>	<b>10</b>
2.1	PocketQube Model . . . . .	10
2.2	Environmental model and assumptions . . . . .	10
2.2.1	Reference frame . . . . .	10
2.2.2	Environmental models . . . . .	12
2.2.3	External disturbances . . . . .	12
2.3	Orbit and attitude kinematic propagators . . . . .	12
2.4	Sensor and actuator models . . . . .	13
2.4.1	Gyroscope . . . . .	13
2.4.2	Photodiodes . . . . .	13
2.4.3	Magnetometer . . . . .	13
2.4.4	Magnetorquer . . . . .	14
2.5	Simulaton / model sampling times and frequencies . . . . .	14
<b>3</b>	<b>Simulation performance campaign plan and results</b>	<b>14</b>
3.1	Nadir Pointing Mode . . . . .	14
3.1.1	Assumptions and limitations . . . . .	14
3.1.2	Nadir pointing results . . . . .	15
3.1.3	Nadir pointing using an External Kalman Filter for attitude determination . . . . .	21
3.2	Detumbling mode . . . . .	29

---

## Acronyms

**BOL** Begin of Life

**CAD** Computer Aided Design

**EOL** End of Life

**ETSETB** Barcelona School of Telecommunications Engineering

**EU** European Union

**FEM** Finite Element Model

**GMM** Geometrical Mathematical Model

**ICD** Interface Control Document

**IR** Infrared

**NOTR** Non-Operational Temperature Ranges

**OTR** Operational Temperature Ranges

**PCB** Printed Circuit Board

**TBD** To be determined/defined

**TCS** Thermal Control System

**TMM** Thermal Mathematical Model

**TRP** Temperature Reference Point

**VCD** Verification Control Document

## List of Figures

2.1	PocketQube 3D model . . . . .	10
2.2	ECI frame representation . . . . .	11
2.3	Body frame representation . . . . .	11
2.4	LVLH frame representation . . . . .	12
3.1	Ground track of the simulated PocketQube orbit . . . . .	15
3.2	Eclipse phases . . . . .	15
3.3	Drag Force (mN) . . . . .	16
3.4	Radiation Force (mN) . . . . .	16
3.5	Aerodynamic Torques . . . . .	16
3.6	Gravity Gradient Torques . . . . .	16
3.7	Radiation Torques . . . . .	16
3.8	Magnetic Torques . . . . .	17
3.9	Gyro data X Axis . . . . .	17
3.10	Gyro data Y Axis . . . . .	17
3.11	Gyro data Z Axis . . . . .	17
3.12	Magnetometer data X Axis . . . . .	17
3.13	Magnetometer data Y Axis . . . . .	17
3.14	Magnetometer data Z Axis . . . . .	17
3.15	Photodiode data . . . . .	18
3.16	Sun position (ECI) X Axis . . . . .	18
3.17	Sun position (ECI) Y Axis . . . . .	18
3.18	Sun position (ECI) Z Axis . . . . .	18
3.19	Magnetic Field (ECI Frame) . . . . .	19
3.20	Attitude Rate . . . . .	19
3.21	Magnetic torque . . . . .	20
3.22	Intensity x Axis . . . . .	20
3.23	Intensity y Axis . . . . .	20
3.24	Intensity z Axis . . . . .	20
3.25	LVLH To Body Quaternion . . . . .	21
3.26	Angle between nadir and +Y . . . . .	21
3.27	Drag Force (mN) . . . . .	22
3.28	Radiation Force (mN) . . . . .	22
3.29	Aerodynamic Torques . . . . .	22
3.30	Gravity Gradient Torques . . . . .	22
3.31	Radiation Torques . . . . .	23
3.32	Gyro data X Axis . . . . .	23
3.33	Gyro data Y Axis . . . . .	23
3.34	Gyro data Z Axis . . . . .	23
3.35	Magnetometer data X Axis . . . . .	23
3.36	Magnetometer data Y Axis . . . . .	23
3.37	Magnetometer data Z Axis . . . . .	23
3.38	Photodiode data . . . . .	24
3.39	Sun position (ECI) X Axis . . . . .	24
3.40	Sun position (ECI) Y Axis . . . . .	24
3.41	Sun position (ECI) Z Axis . . . . .	24
3.42	Attitude Rate . . . . .	25
3.43	Magnetic Torques . . . . .	25
3.44	Intensity x Axis . . . . .	25
3.45	Intensity y Axis . . . . .	25
3.46	Intensity z Axis . . . . .	25
3.47	LVLH To Body Quaternion . . . . .	26
3.48	Quaternion evolution for 20 simulations . . . . .	27
3.49	Performance $q_1$ . . . . .	27
3.50	Performance $q_2$ . . . . .	28
3.51	Performance $q_3$ . . . . .	29
3.52	Performance $q_4$ . . . . .	29

## **List of Tables**

---

## APPROVAL

<b>Title</b> <b>FYS DRD and Guidelines</b>			
Issue Number	1	Revision Number	0
Author		Date	
Approved By		Date of Approval	

## CHANGE LOG

Reason for change	Issue Nr	Revision Number	Date
First release	1	0	
Second release	2	0	

## CHANGE RECORD

<b>Issue Number</b>	<b>Revision Number</b>		
Issue Number	1	Revision Number	0
Reason for change	Date	Pages	Paragraph(s)
First release			
Second release			

---

## DISTRIBUTION

---

### Disclaimer

This document has been prepared for use by the Fly Your Satellite! PoCat Lektron team.

**This document shall be considered confidential and not to be distributed further without permission of  
ESA Education, and the authors.**

---

---

## Applicable Documents

Reference	Document Title	Issue/Release Date
RD01	ECSS-E-ST-31C Space Engineering	Issue 2, 2008/11/15
RD02	ECSS-E-HB-31-01 - Space Engineering - Thermal design handbook - Part 1 to 16	multiple
RD03	P. D.G. Gilmore, "Spacecraft Thermal Control Handbook: Fundamental Technologies", ESA-TEC-MTT	2002

---

# 1 Introduction

The <sup>Po</sup>Cat-Lektron AOCS analysis includes a comprehensive simulation model to support the design, verification, and validation of the attitude and orbit control system for the <sup>Po</sup>Cat-Lektron mission. Developed at the UPC NanoSat Lab as part of the IEEE OpenPocketQube Kit initiative and selected for the ESA Fly Your Satellite! program, the mission comprises two 1P PocketQubes equipped with L-band and K-band radiometers for remote sensing and RFI monitoring.

The simulation campaign evaluates key operational modes, such as Nadir Pointing and Detumbling, assessing performance against mission requirements. Results demonstrate the impact of sensor noise and external disturbances, and highlight the effectiveness of advanced estimation techniques like the Extended Kalman Filter (EKF) in improving attitude determination and meeting pointing accuracy objectives. This simulation framework provides critical insights for the successful implementation of the AOCS in the <sup>Po</sup>Cat-Lektron.

## 1.1 The <sup>Po</sup>Cat-Lektron mission

### 1.1.1 Mission statement

The <sup>Po</sup>Cat-Lektron is a mission resulting from the IEEE OpenPocketQube Kit initiative, developed at the UPC NanoSat Lab. The mission has been selected in the 4th call of the ESA Fly Your Satellite! (FYS) program. The mission analysis presented corresponds to the <sup>Po</sup>Cat-Lektron mission. It consists of two 1P PocketQubes, the PoCat-2 and the PoCat-3, developed as a part of the IEEE OpenPocketQube Kit. This mission aims to demonstrate the feasibility of PocketQube platforms for remote sensing applications.[?]

The payloads on board of the PocketQubes are two passive radiometers to be used for RFI purposes on K and L bands. Apart from the remote sensing nature of the mission, this mission also aims to demonstrate the feasibility of the PocketQube platforms to create, manage and join Federated Satellite Systems. To do so, the FSS Experiment will be reproduced as a part of the experiments of the mission.

### 1.1.2 Mission Objectives

- **Demonstration of Scientific Viability:** Demonstrate the feasibility of conducting scientific missions using PocketQube platforms. To do so, the mission proposes collecting valuable RFI data through a K-Band and L-Band passive radiometers (One for each PocketQube). The payloads will monitor interferences on these bands. This data will facilitate enhanced detection and the generation of heatmaps indicating RFI distribution across the globe. In this experiment we aim to obtain data on the K-Band to see the impact on the atmospheric water vapor measurements, and in the L-Band the interferences over the Position Navigation and Timing (PNT) signals.
- **Satellite Federation Concept:** To establish and demonstrate that PocketQube platforms can create, manage and join Federated Satellite System (FSS). This proof of concept for this resource-limited platforms is based on the reproduction of the FSS Experiment conducted at the UPC NanoSat Lab. The demonstration consist on creating a federation between 2 PocketQubes, in order to download data. Previous missions such as the FSS-Cat from the UPC NanoSat Lab demonstrated the feasibility of this opportunistic collaboration using 6U CubSats.
- **Educational Development:** As a mission developed at the UPC NanoSat Lab, the mission is oriented for undergraduate students to gain experience and get involved in real space missions. In addition, several Bachelor and Master Thesis had been done from this project, apart from the academic papers that this project has produced.

---

## 2 Simulation model

To assist the AOCS design, verification and validation, a simulation model using matlab code has been used. The simulation is based on the Princeton Toolbox [1], which contains a set of functions and simulations initially created for CubeSats, that has been adapted to the PocketQube.

### 2.1 PocketQube Model

The mission is formed by two PQs, one using an L-band Radiometer and the other using a K-band radiometer. To model the PQ, a 3 dimensional cube has been used, shown in *Figure 2.1*. This cube has the same dimensions as a PQ 5x5x5 cm<sup>3</sup> and the same mass as the PQs. Additionally, to apply the inertia of the PQs, the inertia matrix is taken into account in the simulation.

The satellites will be simulated in two different configurations, on the one hand in stowed configuration (without the antennas deployed) and on the other hand in deployed configuration. In the case of the L-band PQ the stowed configuration contains both the L-band antenna and communications antenna stowed.

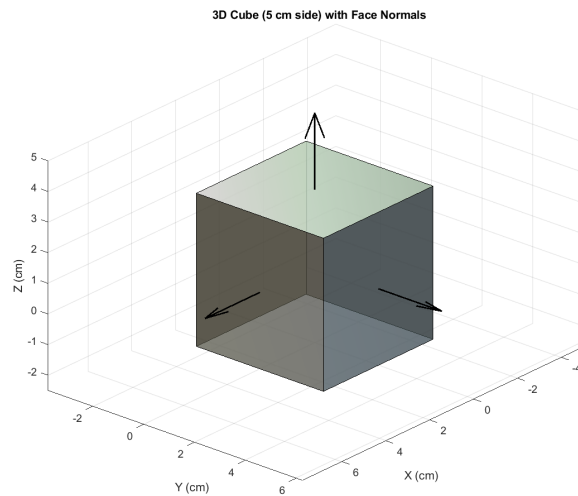


Figure 2.1: PocketQube 3D model

## 2.2 Environmental model and assumptions

### 2.2.1 Reference frame

- **Earth Centered Inertial (ECI) frame:**

The ECI frame is a global cartesian reference frame that has its origin at the centre of the Earth.

- X axis points to the Vernal Equinox.
- Y axis completes the set with the right-hand rule.
- Z axis aligned with the Earth's rotation axis.

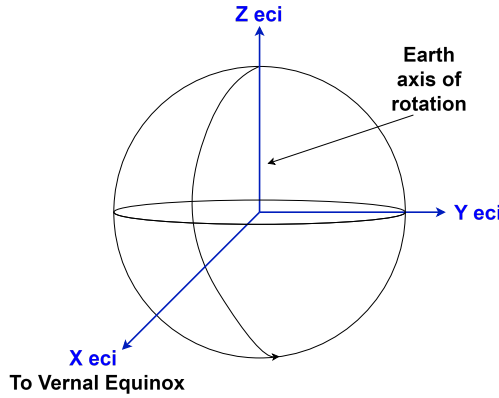


Figure 2.2: ECI frame representation

- **Body frame:**

The Body frame is a global cartesian reference frame that has its origin at the centre of the PQ.

- X axis aligned with the PocketQube width, parallel to the sliding plate and perpendicular to the direction of insertion into the PocketQube deployer.
- Y axis aligned with the PocketQube length, the direction of insertion into the PocketQube deployer and completing the right handed reference frame.
- Z axis aligned with the PocketQube height direction, pointing upwards from the sliding plate.

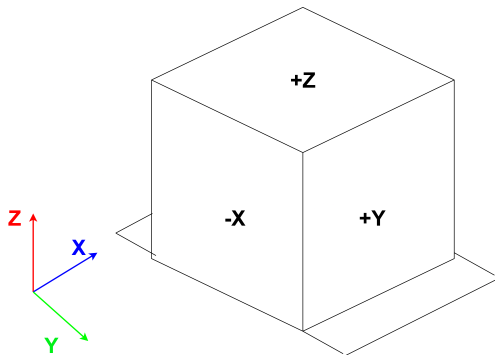


Figure 2.3: Body frame representation

- **Local Vertical Local Horizontal (LVLH) Frame:**

The LVLH Frame will be mainly used for results presentation in the Nadir pointing simulations. The frame is described as:

- X-Axis: Perpendicular to Y and Z, forming a right-handed coordinate system - Local Horizontal
- Y-Axis: Negative to the orbit normal, or in the direction of - $\mathbf{h}$
- Z-Axis: Oriented in the direction of  $-\mathbf{r}$  (points to center of Earth) - Local Vertical

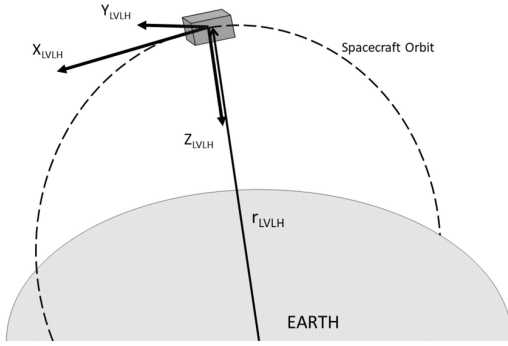


Figure 2.4: LVLH frame representation

### 2.2.2 Environmental models

The following environmental models are used in the simulation:

- **Earth's magnetic field model [2]:** The Earth's magnetic field model used in the simulation is based on the Tilted dipole mode, which includes the effect of the dipole motion of the Earth.
- **Aerodynamic Drag model:** The simulation uses an aerodynamic drag model based on the Jacchia's 1970 model [3].
- **Radiation Pressure model:** The simulation includes the solar radiation pressure, the earth radiation pressure and the earth albedo pressure.
- **Gravity field model:** The simulation accounts for a point-mass gravity model.

### 2.2.3 External disturbances

The following external disturbances are considered in the simulation:

- **Drag force:**
- **Aerodynamic torques:**
- **Gravity gradient torques:**
- **Radiation Torques:**

## 2.3 Orbit and attitude kinematic propagators

As for the Orbit propagator in the simulation, firstly, the used equations of motion are the Cowell' form of the two body problem, using disturbances. In addition, the integrator type used is the Runge-Kutta 4th order method. As for the propagation of the parameters, they are done in the Earth Centered Inertial (ECI) frame.

The parameters included in the initial vector for describing the state of the satellite at the begining of the simulation are:

- Satellite's position.
- Satellite's velocity.
- Satellite's attitude quaternion.
- Satellite's angular velocity.

Regarding the attitude representation of the satellite in the simulation, the mathematical expression that will be used is the quaternion. During the simulation the quaternion that will be used is the one representing the rotation from the body frame to the ECI frame. However, at the time to present the results the quaternion that will be used will be the one representing a rotation from the Local Vertical Local Horizontal (LVLH) frame to the ECI frame.

## 2.4 Sensor and actuator models

In this section all the models used for the sensors and for the actuators are described. It is assumed that all the sensors have been calibrated and temperature characterized. A brief list of the sensors and actuators included in the PQ is presented below:

Sensors	Actuator
Gyroscope	Magnetorquer
Photodiodes	
Magnetometer	

### 2.4.1 Gyroscope

The model used to represent the gyroscope output given by [4] is:

$$\omega = \omega_o + b(t) + n, \quad (1)$$

where:

- $\omega$  is the measured angular velocity vector.
- $\omega_o$  is the true angular velocity of the satellite.
- $b$  is the bias term, modeled as a random walk process.
- $n$  is a zero-mean Gaussian noise vector.

### 2.4.2 Photodiodes

The output of the photodiodes can be modeled as:

$$v = v_o(T) + n \quad (2)$$

where:

- $v$  is the measured voltage output vector,
- $v_o(T)$  is the true signal component that is dependent to the temperature  $T$  previously calibrated.
- $n$  represents additive noise, typically modeled as zero-mean Gaussian noise.

### 2.4.3 Magnetometer

The magnetometer model is expressed as:

$$\mathbf{B}_{\text{meas}} = (\mathbf{C}_e \cdot \mathbf{B}_{\text{true}}) + \mathbf{b}_e + n \quad (3)$$

where:

- $\mathbf{B}_{\text{meas}}$  is the measured magnetic field vector in the body frame.
- $\mathbf{B}_{\text{true}}$  is the true magnetic field vector in the body frame.
- $\mathbf{C}_e$  is the calibration matrix with errors.
- $\mathbf{b}_e$  is the sensor bias error vector.
- $n$  is zero-mean Gaussian white noise with known variance.

#### 2.4.4 Magnetorquer

The magnetorquers are simulated as a mathematical formula. The magnetorquers generate a magnetic moment depending on the injected intensity, therefore, in the simulation this magnetic moment is calculated and later used to propagate the following attitude of the satellite with the other external disturbances. The formula used for calculating the magnetic moment generated by the magnetorquers is:

$$\mathbf{m} = I_o N_{layers} \sum_{i=1}^{N_{turns}} (l - 2(i-1)(w+d))^2 \quad (4)$$

Where the  $l$  is the length of the magnetorquer, the  $w$  the width of the copper trail, the  $d$  the distance between trails,  $N_{layers}$  is the number layers in which the magnetorquer is divided and  $N_{turns}$  is the number of turns in the magnetorquer. The  $I_o$  is the injected current, which is the input of the magnetorquer. The table below shows the characteristics of the magnetorquers used in the simulation:

Board	Turns	Max moment ( $\text{A}\cdot\text{m}^2$ )	Dimensions ( $\text{mm} \times \text{mm}$ )	Layers
Top	$42 \times \text{layer}$	$9.17 \times 10^{-4}$	$32 \times 32$	4
Bottom & Lateral	$38 \times \text{layer}$	0.0017	$32 \times 32$	4

## 2.5 Simulaton / model sampling times and frequencies

The simulation time used is 2 seconds which corresponds to 0.5 Hz. This is due to the fact that the on board computer (OBC) used in the PQ only has one thread to manage all the tasks, therefore, the sampling frequency has been chosen thinking in the worst case scenario. The sampling time of the sensors is the same one as the simulation time.

# 3 Simulation performance campaign plan and results

In this section the simulation results of the two different operational modes of the ADCS in the PQ are presented.

## 3.1 Nadir Pointing Mode

The objective of the Nadir Pointing is to point the Payload located at the top board of the PocketQube towards the Earth, so that the Payload can take measurements of the Earth. For this mode the following requirements have been defined:

*The Absolute Performance Error (APE) of the Payload boresight shall be less than 20° with respect to the Y and X axes, which are the axes perpendicular to the boresight, and this requirement should be met for 95% of the time.*

### 3.1.1 Assumptions and limitations

The list below presents the different assumptions and aspects considered to perform the simulations.

- **Orbit parameters**

- Inclination: 90 degrees
- Altitude: 500 Km
- Eccentricity: 0 degrees
- Initial satellite position: [ 6887 , 0 , 0 ] Km
- Initial satellite velocity: [ 0 , 0 , 7.6 ] Km/s

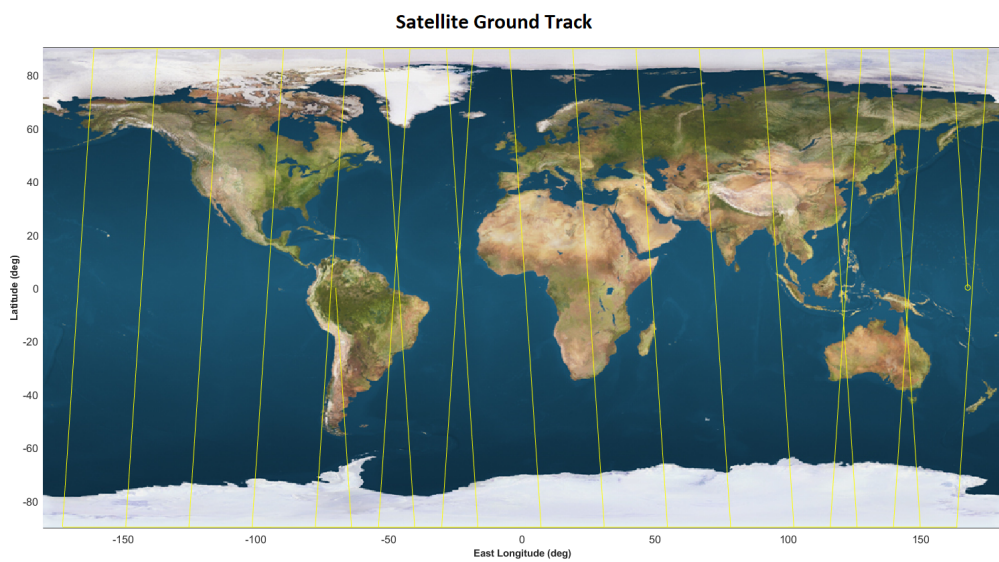


Figure 3.1: Ground track of the simulated PocketQube orbit

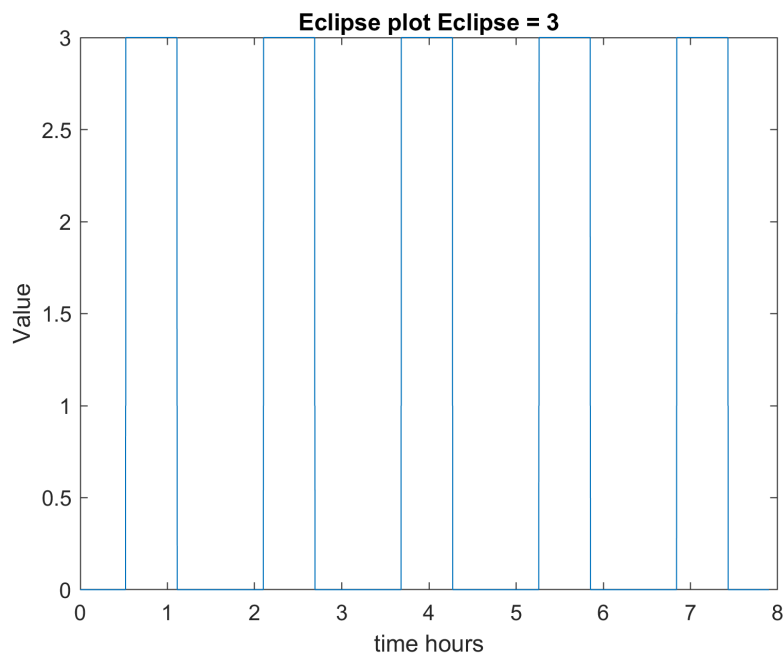


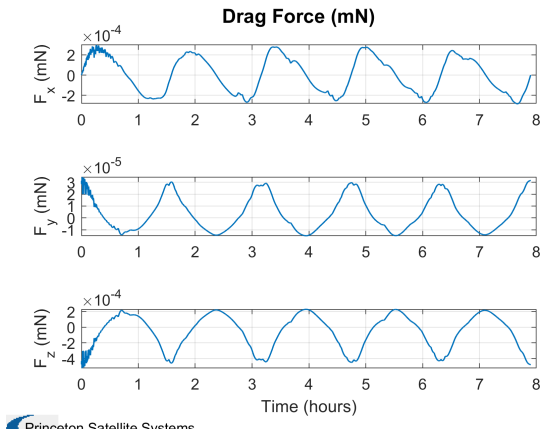
Figure 3.2: Eclipse phases

- **Number of simulated orbits:** 10 orbits
- **Simulation starting date:** 05/04/2027 00:00:00 UTC
- **Simulation time step:** 2 seconds

### 3.1.2 Nadir pointing results

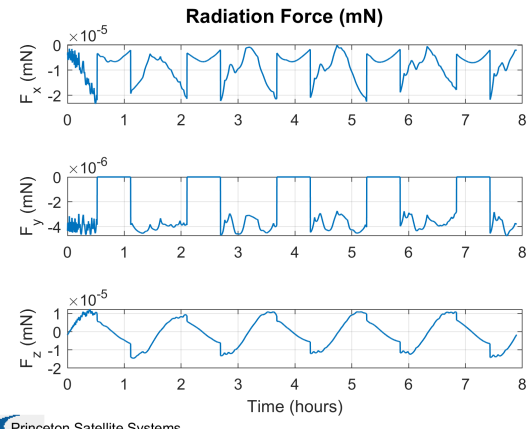
- **External perturbations**

In the following plots, the values of the different external perturbations affecting the simulation are shown.



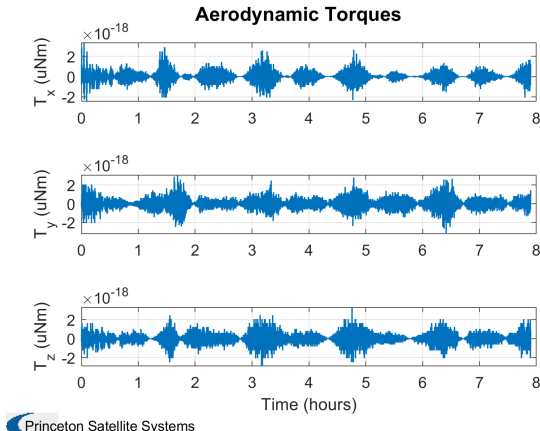
Princeton Satellite Systems

Figure 3.3: Drag Force (mN)



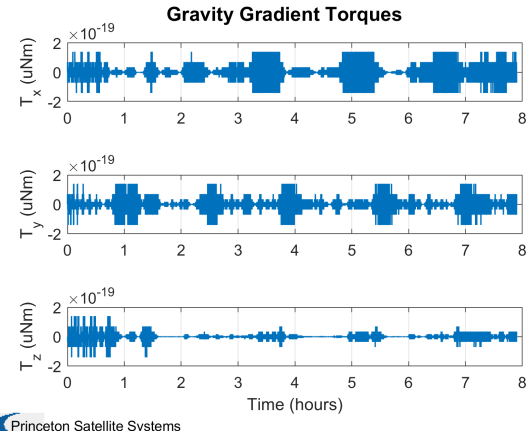
Princeton Satellite Systems

Figure 3.4: Radiation Force (mN)



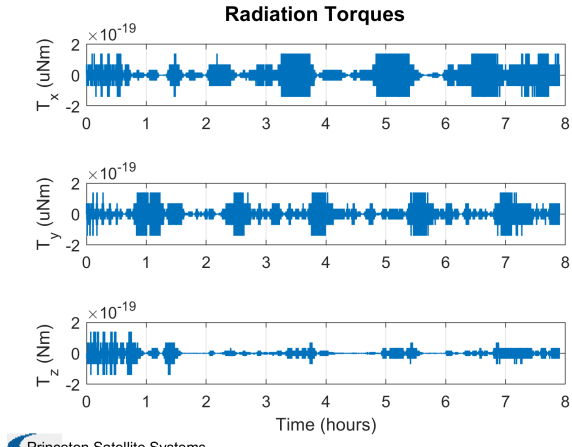
Princeton Satellite Systems

Figure 3.5: Aerodynamic Torques



Princeton Satellite Systems

Figure 3.6: Gravity Gradient Torques



Princeton Satellite Systems

Figure 3.7: Radiation Torques

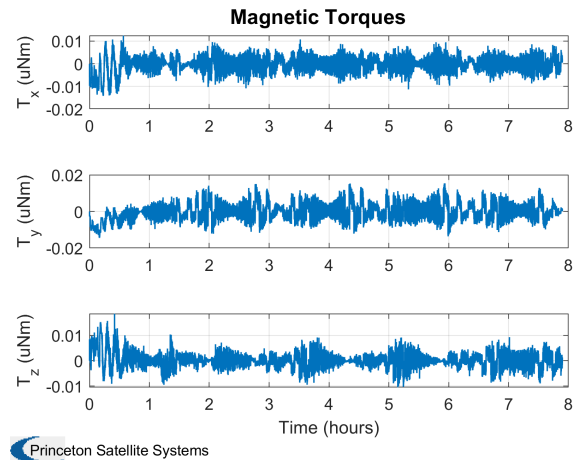


Figure 3.8: Magnetic Torques

- **Sensor measurements**

In this section the measures taken from the simulated sensors are presented. The sensors follow the model presented in the previous sections of the document. Firstly the measurements of the gyroscope are presented, it can be observed the effect that the noise and the random walk phenomenon has on the measures. It can also be observed how the Nadir Pointing controller first tries to conduct a little detumbling functionality in order to reduce the angular velocity as much as possible. This effect can be observed in the first hour of the simulation.

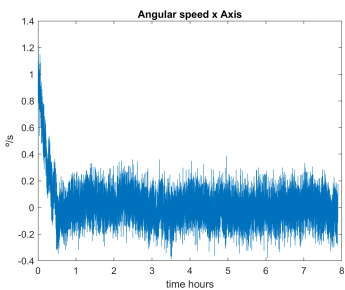


Figure 3.9: Gyro data X Axis

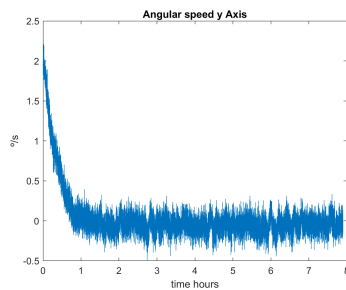


Figure 3.10: Gyro data Y Axis

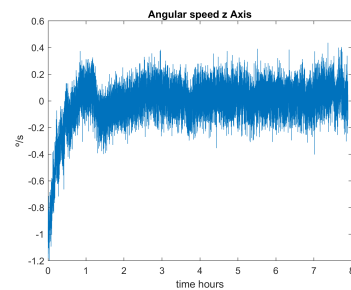


Figure 3.11: Gyro data Z Axis

Secondly, in the following pictures the magnetic field measured by the magnetometer is shown.

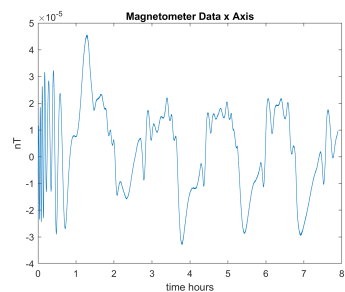


Figure 3.12: Magnetometer data X Axis

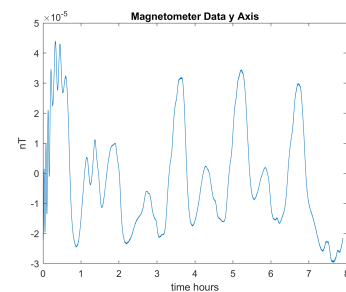


Figure 3.13: Magnetometer data Y Axis

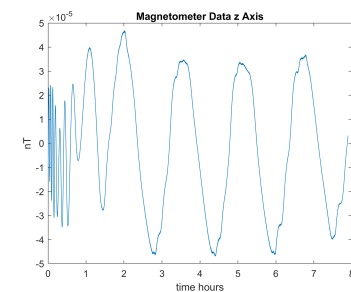


Figure 3.14: Magnetometer data Z Axis

Finally, the last plot of the sensors includes the measurements of all 6 photodiodes used in the satellite. Each axis of the PocketQube corresponds to the following number: 1 to +Z, 2 to -Z, 3 to +X, 4 to +Y, 5 to -X and 6 to -Y.

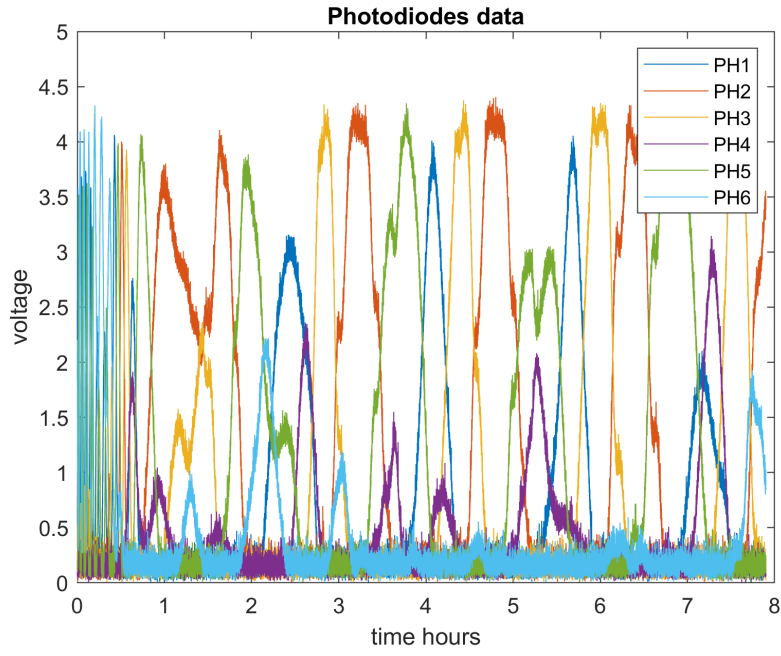


Figure 3.15: Photodiode data

- **Sun Position Algorithm Performance**

In the following section the performance of the developed Sun position algorithm estimator that uses the photodiodes and the temperature sensors is presented. The plots show two different lines, on the one hand an orange line which indicates the real position of the sun, and on the other hand a blue line which indicates the estimation of the algorithm. It can be observed that the performance of the estimation is degradated by the noise of the photodiodes, the less noise the better estimation.

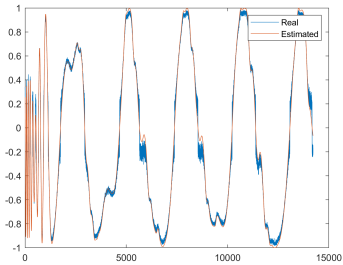


Figure 3.16: Sun position (ECI) X Axis

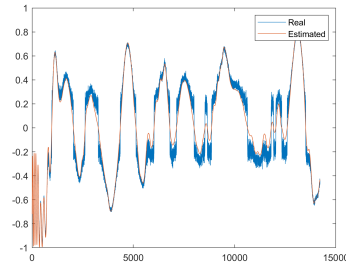


Figure 3.17: Sun position (ECI) Y Axis

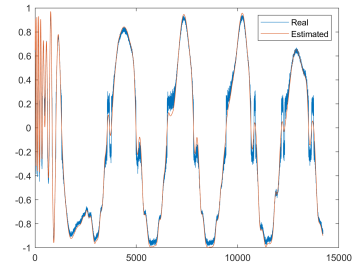
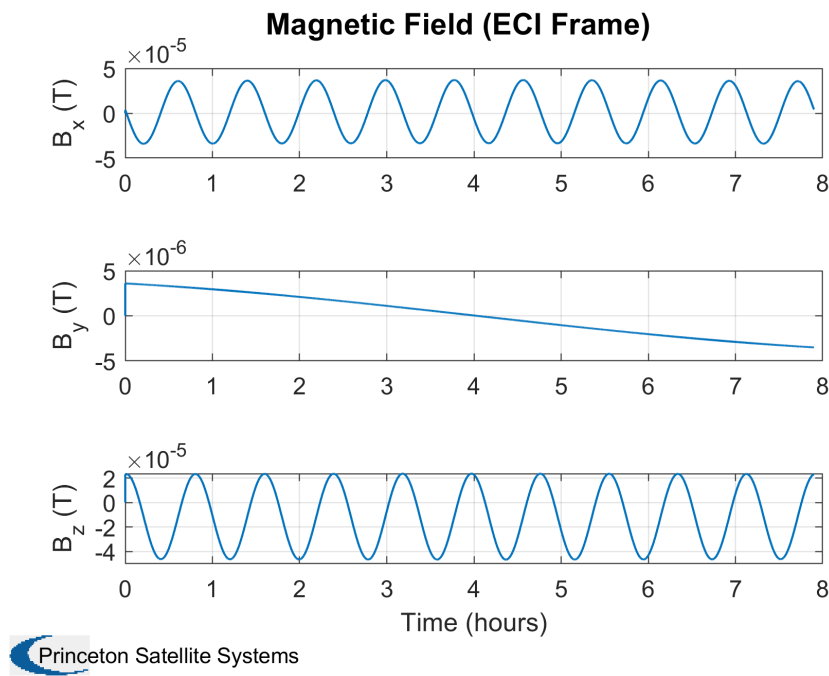


Figure 3.18: Sun position (ECI) Z Axis

- **Magnetic Field Model**

In this section the propagated magnetic field over the simulation is presented. The model as explained in the previous sections is based on the tilted dipole model to reduce as much as possible the simulation time.

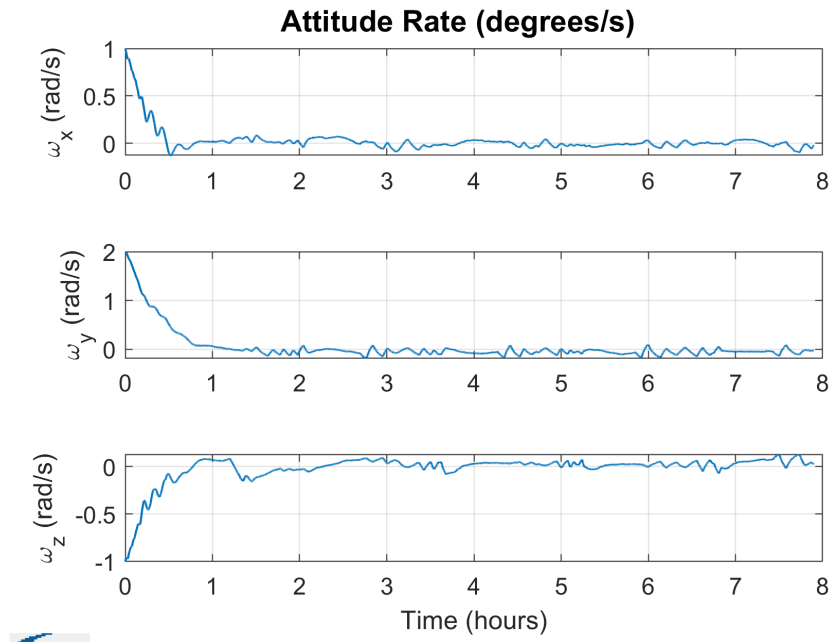


 Princeton Satellite Systems

Figure 3.19: Magnetic Field (ECI Frame)

- **Real angular Velocity**

In the following plot it is shown the angular velocity propagated in each iteration of the simulation. In short words it is the real angular velocity in which the satellite is rotating due to the torques affecting the PocketQube.

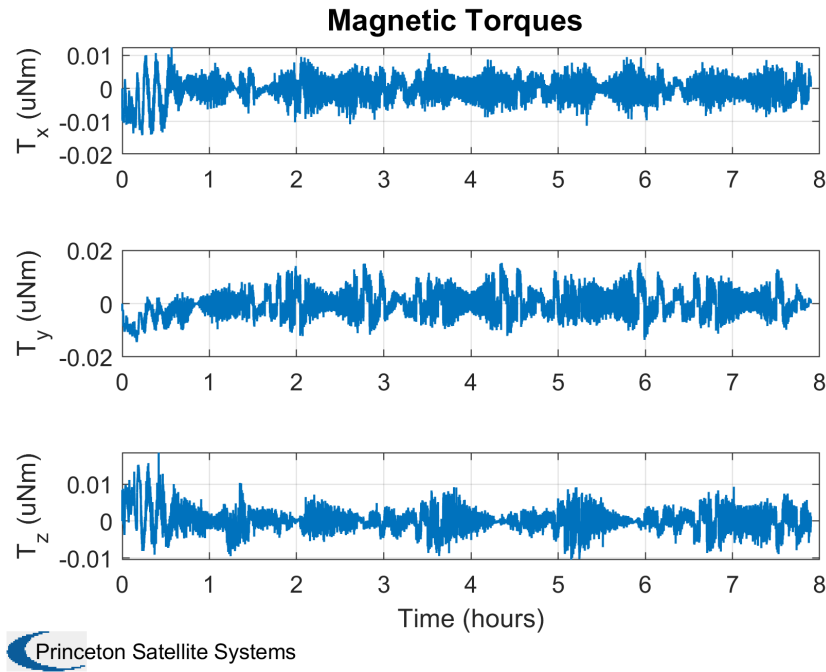


 Princeton Satellite Systems

Figure 3.20: Attitude Rate

- **Generated torque**

In the pictures below it is observed the generated torque by the magnetic moment generated by the magnetorquers. This torque is the required torque to be applied in order to conduct the Nadir Pointing mode.



 Princeton Satellite Systems

Figure 3.21: Magnetic torque

- **Injected Intensity**

The following plots show the required intensity to be injected in the magnetorquers in order to generate the necessary magnetic moment to conduct the Nadir Pointing mode. It can be observed that the intensity is quantified due to the limitations of the magnetorquer driver, as it can only inject from 0.5 mA to 32 mA in steps of 0.5 mA. If the computed intensity exceeds the maximum value, the simulation limits this intensity to 32 mA, as can be seen in the first hour of the simulation.

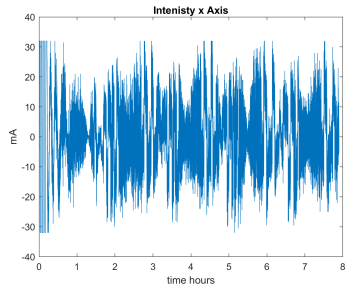


Figure 3.22: Intensity x Axis

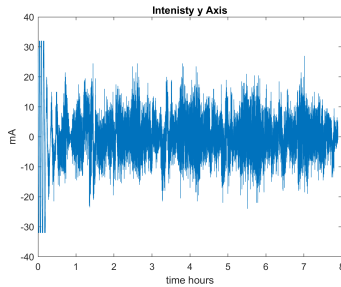


Figure 3.23: Intensity y Axis

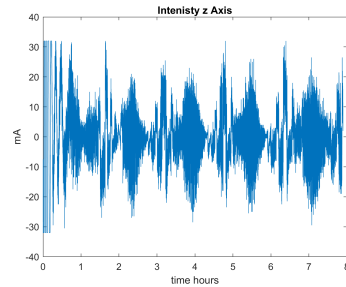
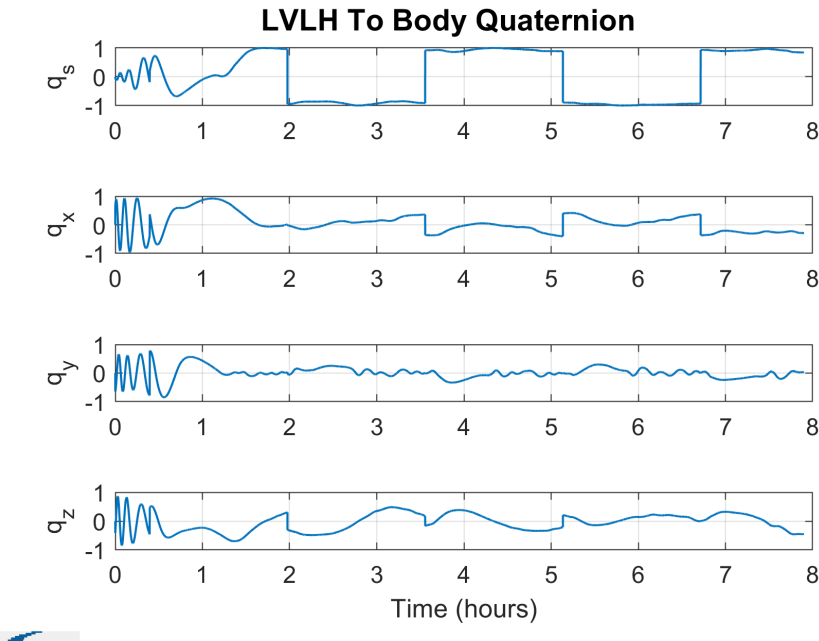


Figure 3.24: Intensity z Axis

- **Attitude quaternion**

The following plot indicates the attitude quaternion of the PocketQube. The selected quaternion is the one representing the rotation from the Local Vertical Local Horizontal (LVLH) frame to the body frame. This quaternion is selected to show the performance of the Nadir Pointing mode, as the quaternion indicating that the PQ is pointing to the Nadir angle has a very simple representation, which is the quaternion  $[+/-1, 0, 0, 0]$ . In the plot can be observed that the scalar component ( $q_s$ ) of the quaternion of the PQ is de desired one. Nevertheless, the vectorial part is where can be observed the effect of the noise of the sensors and the errors in the estimations, they do not converge exactly to zero; instead, residual errors remain, resulting in some inaccuracy in the pointing.



 Princeton Satellite Systems

Figure 3.25: LVLH To Body Quaternion

In the picture below can be observed the angle between the nadir vector and the +Z unitary vector of the body frame. Additionally, there is a line marking the  $20^\circ$  limit, which is the requirement of the Nadir Pointing mode. Overall, the results show that the requirement is not met, therefore, a solution to improve the performance has to be implemented. The proposed solution is the implementation of an Extended Kalman Filter (EKF) to improve the attitude estimation, which will be presented in the next section.

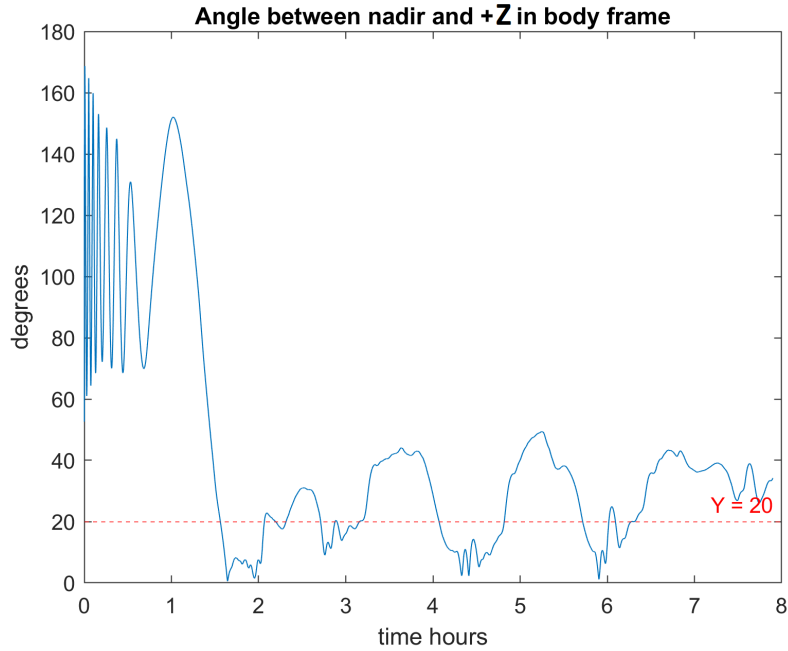


Figure 3.26: Angle between nadir and +Y

### 3.1.3 Nadir pointing using an External Kalman Filter for attitude determination

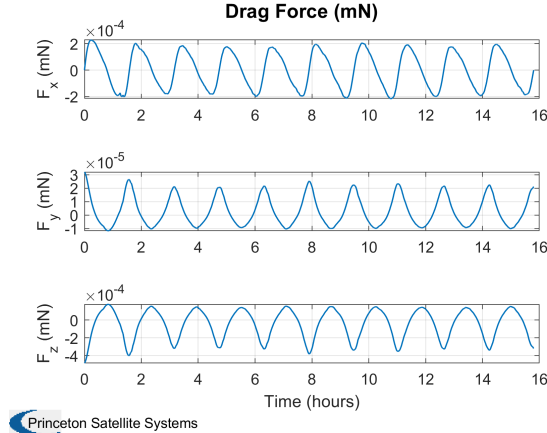
In consequence of the results obtained in the previous seconds, the proposed solution to achieve the requirement of the Payload is to implement an Extended Kalman Filter (EKF) to improve the attitude estimation. The Extende

Kalman Filter used is the one proposed in [5]. This proposed EKF uses the manifold theory to update the attitude quaternion, the covariance matrix of the state and the angular velocity. Additionally, it uses measurements from the gyroscope and the magnetometer to update the state of the EKF.

In this section the results of the simulation of the Nadir Pointing using the EKF are presented. In addition, the performance of the EKF is analysed and compared with the performance of the Nadir Pointing mode without the EKF.

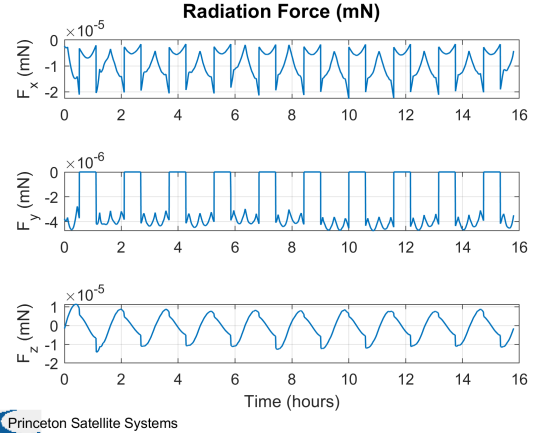
- **External perturbations**

In this section all the external perturbations affecting the PQ are presented.



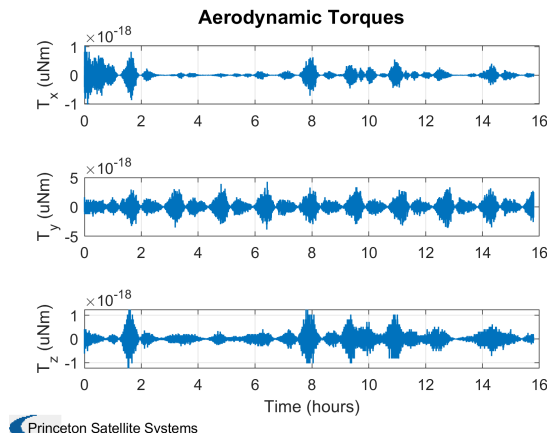
Princeton Satellite Systems

Figure 3.27: Drag Force (mN)



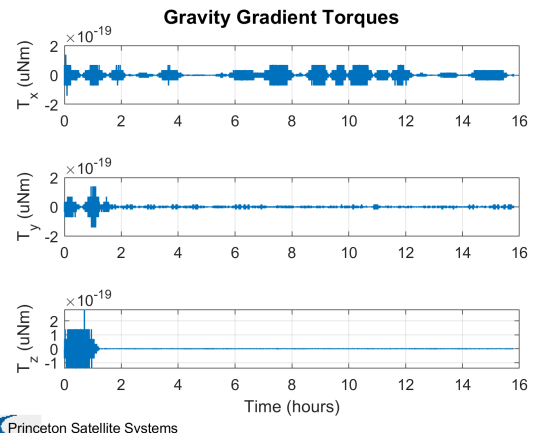
Princeton Satellite Systems

Figure 3.28: Radiation Force (mN)



Princeton Satellite Systems

Figure 3.29: Aerodynamic Torques



Princeton Satellite Systems

Figure 3.30: Gravity Gradient Torques

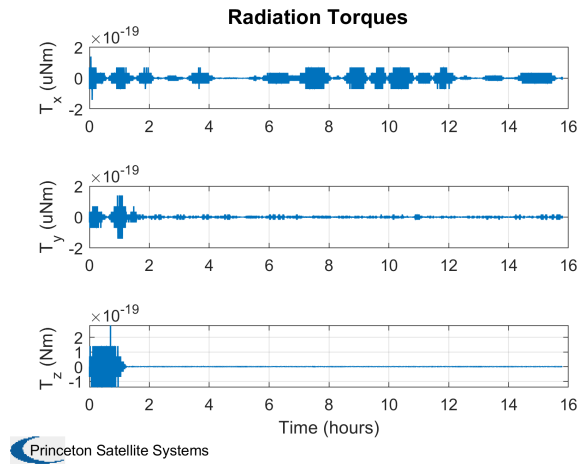


Figure 3.31: Radiation Torques

- **Sensor measurements**

In this section a s in the previous simulation, the sensor measurements are presented. Firstly, the gyroscope measurements are shown.

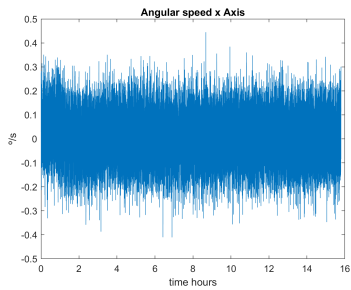


Figure 3.32: Gyro data X Axis

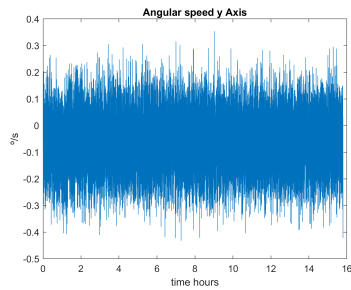


Figure 3.33: Gyro data Y Axis

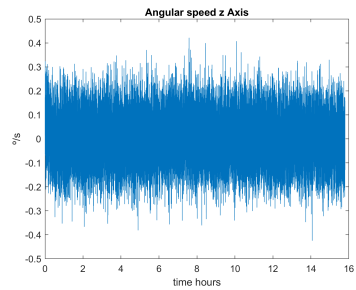


Figure 3.34: Gyro data Z Axis

Secondly, the magnetometer measurements are presented.

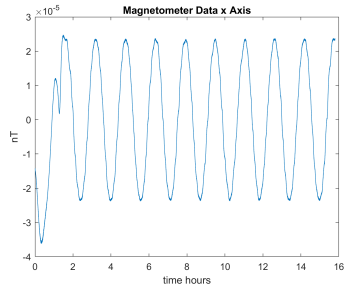


Figure 3.35: Magnetometer data X Axis

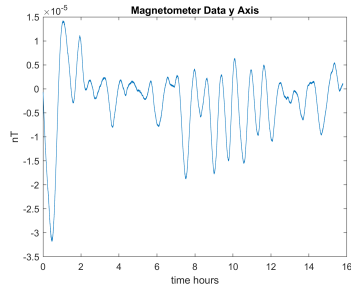


Figure 3.36: Magnetometer data Y Axis

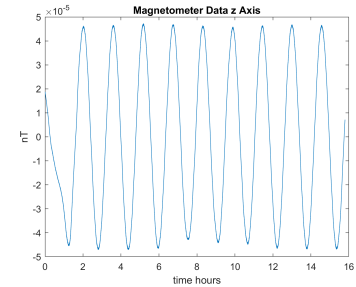


Figure 3.37: Magnetometer data Z Axis

Finally, the photodiode measurements are presented. As in the previous simulation, each axis of the PocketQube corresponds to the following number: 1 to +Z, 2 to -Z, 3 to +X, 4 to +Y, 5 to -X and 6 to -Y.

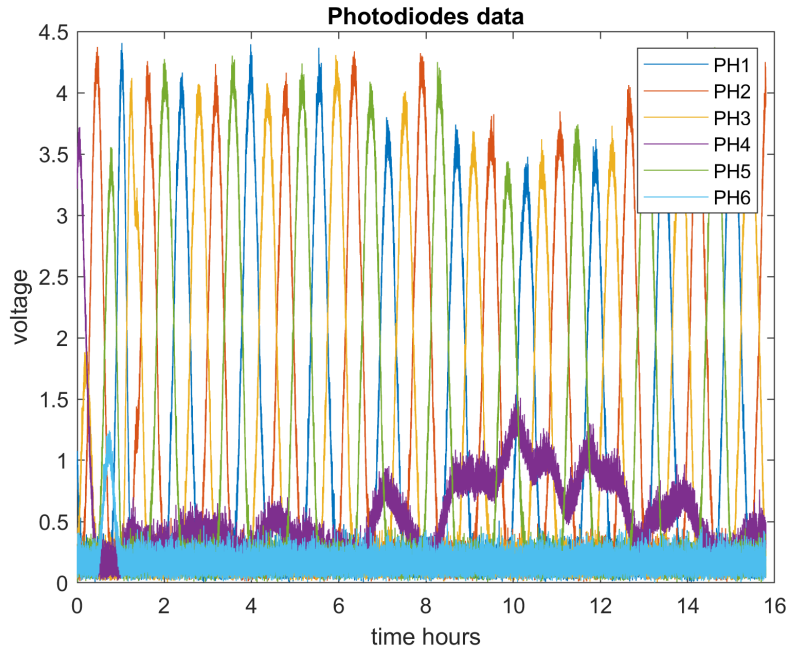


Figure 3.38: Photodiode data

- **Sun Position Algorithm Performance**

In this section the performance of the developed Sun position algorithm estimator that uses the photodiodes and the temperature sensors is presented. Remember that the orange line indicates the real position of the sun, and the blue line indicates the estimation of the algorithm.

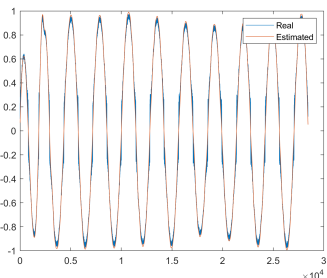


Figure 3.39: Sun position (ECI) X Axis

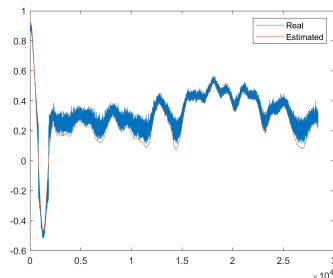


Figure 3.40: Sun position (ECI) Y Axis

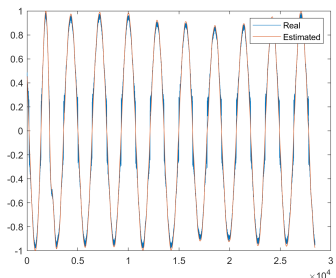


Figure 3.41: Sun position (ECI) Z Axis

- **Real angular Velocity**

This section presents the angular velocity propagated in each iteration of the simulation.

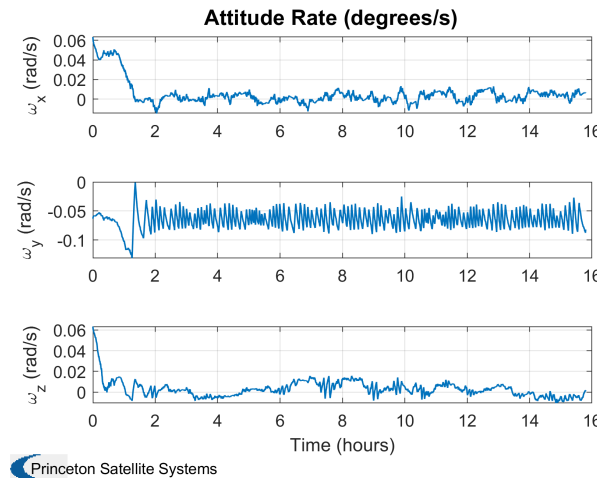


Figure 3.42: Attitude Rate

- **Generated torque**

The following plot shows the generated torque by the magnetic moment generated by the magnetorquers.

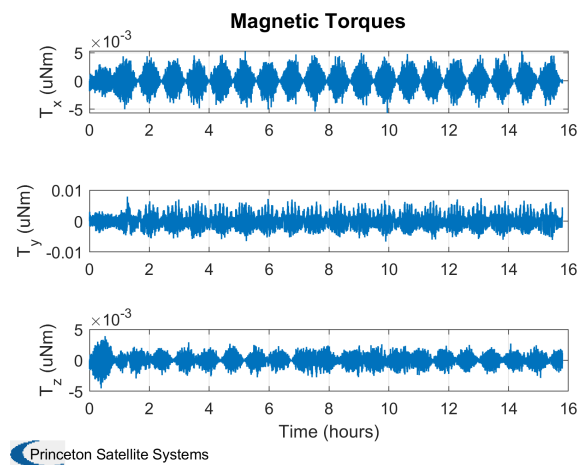


Figure 3.43: Magnetic Torques

- **Injected Intensity**

This section illustrates the required intensity to be injected in the magnetorquers in order to generate the necessary magnetic moment to conduct the Nadir Pointing mode.

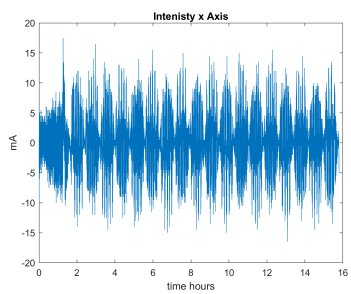


Figure 3.44: Intensity x Axis

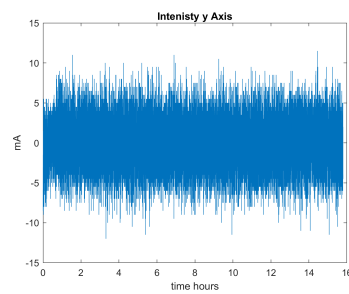


Figure 3.45: Intensity y Axis

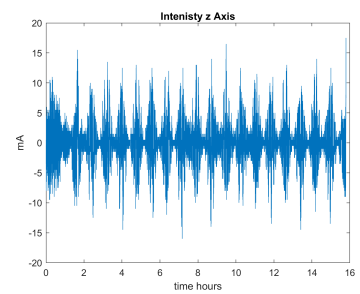


Figure 3.46: Intensity z Axis

- **Attitude quaternion**

In this section the attitude quaternion of the PocketQube estimated by the EKF is presented. A comparative

between the quaternion estimated by the EKF and the quaternion estimated by the simulation without the EKF will be presented in later sections.

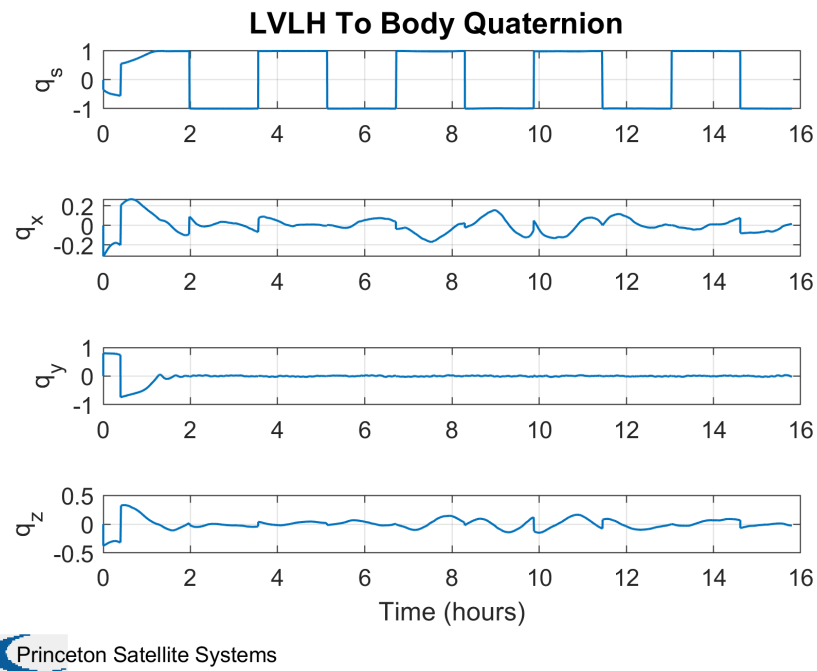


Figure 3.47: LVLH To Body Quaternion

- **EKF Performance**

To assess the performance of the EKF, a performance campaign has been conducted. The campaign consists of 20 simulations using the same initial state and orientation of the PocketQube. After each simulation the orientation of the PocketQube is extracted by means of the quaternion describing the rotation from the Local Vertical Local Horizontal (LVLH) frame to the body frame. Finally that quaternion is used to calculate the mean square error (MSE) of each quaternion component, so that the performance of the EKF can be evaluated. In order to compute the MSE, the ideal quaternion used is the quaternion [1, 0, 0, 0], which represents the ideal attitude of the PocketQube in the Nadir Pointing mode.

The first plot shows the quaternion evolution for the 20 simulations, where it can be observed that in overall, all the quaternion components manage to converge approximately to the ideal quaternion.

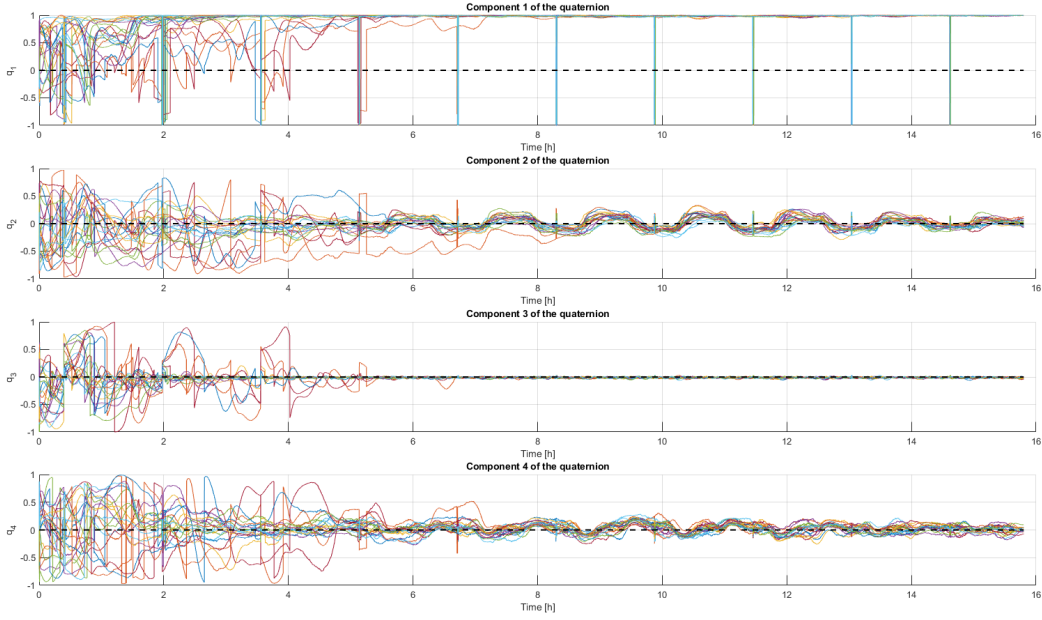


Figure 3.48: Quaternion evolution for 20 simulations

The following plots show the MSE of each quaternion component. Additionally, the bias<sup>2</sup>, the variance and the first component of the covariance matrix are also presented.

In the first plot, the component  $q_1$  of the quaternion is presented, which is the scalar component of the quaternion. In this case, it can be observed that the variance is in most of the plot with a very approximated value to the MSE. That means that the EKF in that component is working extremely close the optimal estimator. It is good to take into account that as an EKF is being used, the fact of having to linearize the system makes complex to obtain an ideal optimal estimator (variance = MSE).

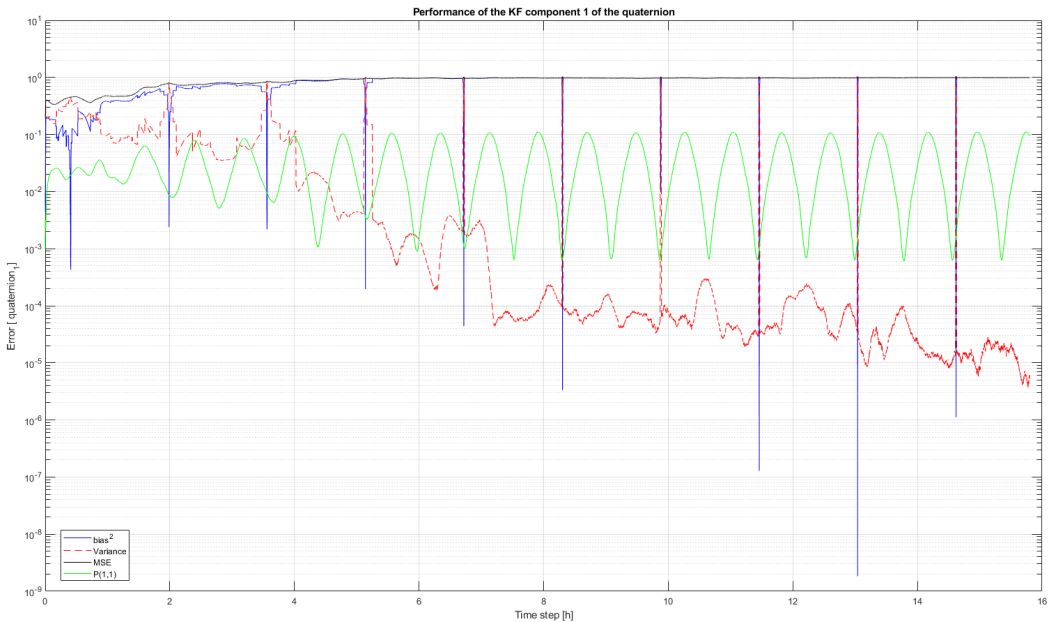


Figure 3.49: Performance  $q_1$

In the following three plots, the components  $q_2$ ,  $q_3$  and  $q_4$  of the quaternion are presented. In this case these components are more valuable for obtaining a better nadir pointing performance. Firstly, in all plots can be observed two different phases, on the one hand, the first phase in which the EKF tries to reduce the angular velocity to 0 and tries to point as close as possible to the nadir vector. In this phase the EKF as can be seen works as the optimal estimator, as the variance is very close to the MSE. This happens because the EKF detects that the covariance matrix varies in time, thus the EKF tries to reduce the MSE and as a consequence the variance to achieve a more constant covariance matrix. In order to do that, the EKF assigns more confidence in the measurements than in the predictions.

In the second phase, once the angular velocity has been significantly reduced and the attitude has converged near the nadir direction, the EKF enters a tracking or steady-state phase. At this point, the estimation no longer requires aggressive corrections. This is reflected in the covariance matrix, which becomes more stable and varies less over time. Since the EKF assumes the system is already well-aligned with the nadir direction, it relies more heavily on its predictions rather than the incoming measurements.

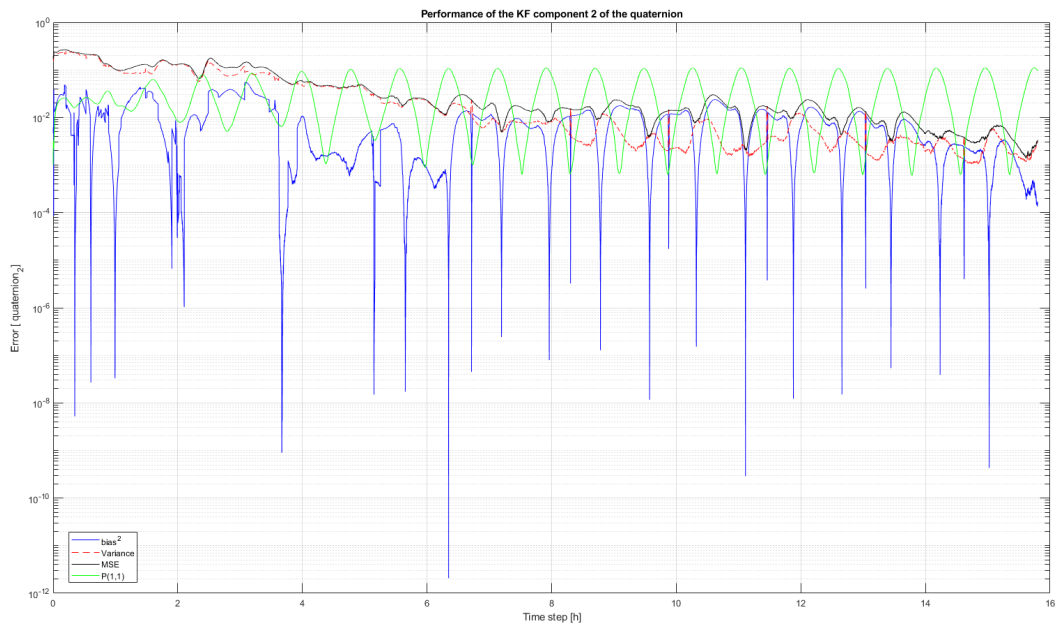


Figure 3.50: Performance  $q_2$

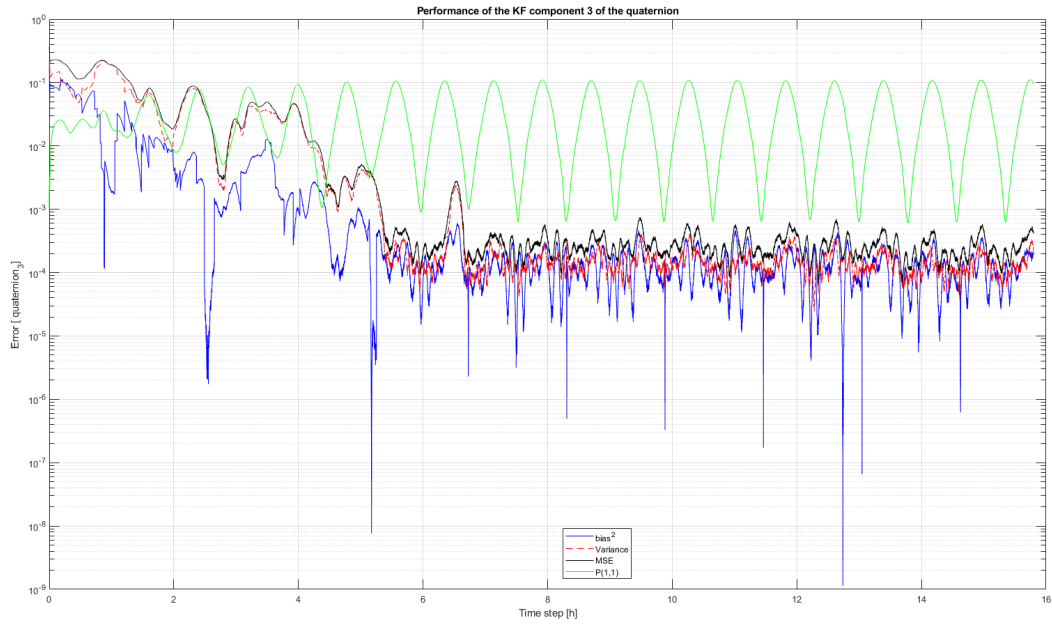


Figure 3.51: Performance  $q_3$

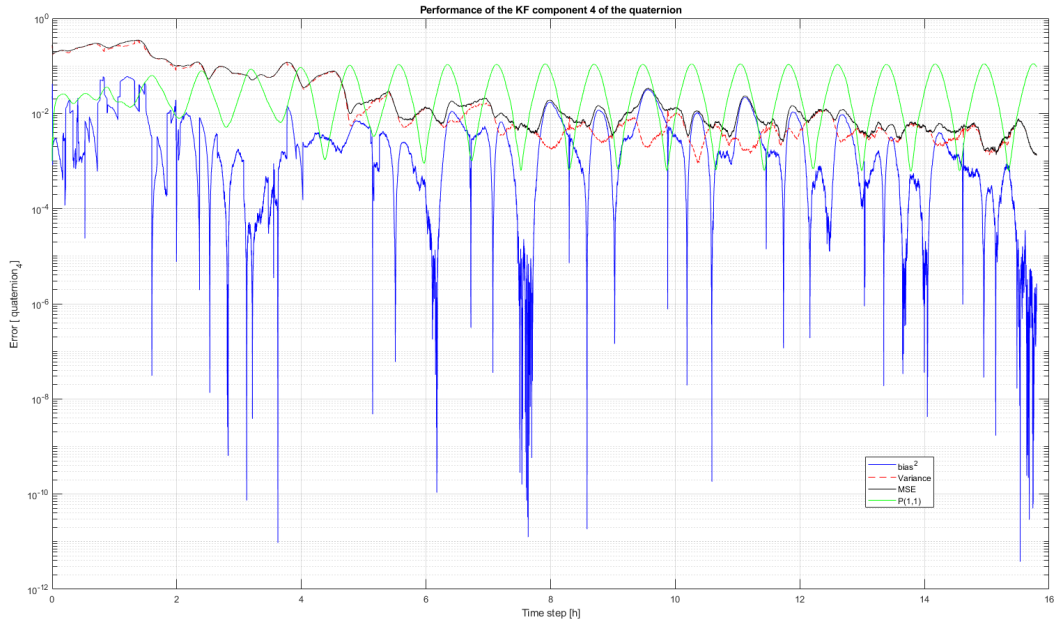


Figure 3.52: Performance  $q_4$

### 3.2 Detumbling mode

---

## References

- [1] Princeton University. Created toolboxes. <https://psatellite.com/>, 2017.
- [2] Wikipedia. Dipole model of the Earth's magnetic field. [https://en.wikipedia.org/wiki/Dipole\\_model\\_of\\_the\\_Earth%27s\\_magnetic\\_field](https://en.wikipedia.org/wiki/Dipole_model_of_the_Earth%27s_magnetic_field), 2025.
- [3] Johnson,D.L and Smith, R.E. The MSFC/J70 orbital atmosphere model and the data bases for the MSFC solar activity prediction technique. <https://ntrs.nasa.gov/citations/19860012552>, 1985.
- [4] F. L. Markley and J. L. Crassidis,. Fundamentals of Spacecraft Attitude Determination and Control, 2014.
- [5] Bernal-Polo, P.; Martínez-Barberá,. Kalman Filtering for Attitude Estimation with Quaternions and Concepts from Manifold Theory. <https://doi.org/10.3390/s19010149>, 2019.